Acta Scientiarum
http://periodicos.uem.br/ojs
ISSN on-line: 1807-8664
Doi: 10.4025/actascitechnol.v43i1.48914

Effect of the ionic radius on structural properties of orthochromites $RCrO_3$ (R = La, Gd, Y)

Romualdo Santos Silva Junior*

Departamento de Física, Universidade Federal de Sergipe, Av. Marechal Rondon, s/n, 49100-000, Jardim Rosa Elze, São Cristóvão, Sergipe, Brazil.
*Author for correspondence. E-mail: romu.fisica@gmail.com

ABSTRACT. The main objective of this work was to detail out how to obtain important parameters in the structural analysis of materials with perovskite structure in order to help beginning researchers in this area. In particular, a thorough comparative and investigative study of the effect of ionic radius on the structural properties of orthochromites $RCrO_3$ (R = La, Gd, Y) were presented. It is observed that the *b* and *c* lattice parameters increased, whereas *a* lattice parameter decreased as the ionic radius increased. Consequently, an increase in the unit-cell volume and tolerance factor was observed. The angles and bond lengths increased with an increase in the ionic radius, albeit the inclination angle, as well as the rotation angle, tends to decrease. The distortion parameter suffered a fluctuation in its value according to the increasing ionic radius. Lastly, Williamson-Hall (W-H) analysis caused a decrement in the strain according to decreasing ionic radius.

Keywords: ionic radius; orthochromites; structural properties.

Received on July 28, 2019.
Accepted on July 3, 2020.

Introduction

An important feature of ABO_3-type perovskites is undoubtedly its ability to couple several properties in their crystalline structure that is, many of its properties can be modified by changing the rotations and distortions of the BO_6 octahedron (Warshi et al., 2018). Distortions and rotations are directly related to the B-O-B bond angles and B-O bond lengths. In fact, the slopes and distortions of octahedral in perovskites are responsible for the control of various physical properties, such as structural transitions and magnetic properties, amongst others (Oikawa, Kamiyama, Hashimoto, Shimojyo, & Morii, 2000; Silva, Aguiar, & Barrozo, 2018).

Recently, the orthochromites $RCrO_3$ have attracted attention owing to their valuable multifunctional properties, for example, the coexistence of magnetism and ferroelectricity with great potential in a spintronic application (Jara, Carvalho, Júnior, Maia, & Santana, 2018), reverse magnetization, exchange bias, and magnetocaloric effect, for application in data storage and magnetic refrigeration (Rajeswaran, Khomskii, Zvezdin, Rao, & Sundaresan, 2012; Zhang et al., 2017), among others. In this sense, for the understanding of the physical properties related to the system $RCrO_3$, it is of fundamental importance to investigate the parameters of structural distortion with great precision. Thus, it is important to note that the rotation of the CrO_6 octahedron through the inclination angles (θ) along the direction [100] and rotation Φ along the direction [010] can be estimated using lattice constants and through the atomic coordinates of oxygen anions (Warshi et al., 2018).

Many works did not emphasize their detailed analysis, let alone comprehensive detailing of the structural properties of the materials studied for more in-depth analysis and applications. Thus, in this paper, we intend to present a detailed comparative and investigative study of the ionic radius effect, on the structural properties of orthochromites $RCrO_3$ (R = La, Gd, Y) such as lattice parameters, atomic positions, inclination angles, rotation angles, bond length, tolerance factor and deformation of the crystalline lattice, with the objective of helping new researchers in this area.

Material and Methods

The parameters used in this work were imported from Inorganic Crystallographic Structure Database (ICSD) for the $LaCrO_3$ (793440), $GdCrO_3$ (251088), and $YCrO_3$ (251108) structures, respectively. Next, we show how the parameters analyzed in this work were extracted. Figure 1 shows the ABO_3 type

orthorhombic perovskite unit cell with A-site cation at the corners and B-site cation at the center surrounded by six oxygen atoms located at the face centers to form the oxygen octahedral. In this work, A-site accommodates La, Gd and Y elements, and B-site the Cr element. The rotation of oxygen octahedral about the three cubic axes (100), (010), and (111) by the angles θ, ϕ, and φ, respectively, can accommodate the deviations from this basic structure (Warshi et al., 2018), as shown in Figure 1(a). The orthochromites $RCrO_3$ (R = La, Gd, and Y) have an orthorhombic symmetry with space group 62 (Pnma) which is a pseudo-cubic space group, and the unit cell parameters are related to the ideal cubic perovskites as $a \cong \sqrt{2}a_p$, $b \cong 2a_p$ and $c \cong \sqrt{2}a_p$, at where a_p is the cubic perovskite cell parameter, with the Wyckoff positions of atoms being: R: 2a (x,1/4,z), Cr: 4b (0,0,1/2), O(1): 4c (x,1/4,z) and O(2): 8d (x,y,z) (Romero, Escamilla, Marquina, & Gómez, 2015).

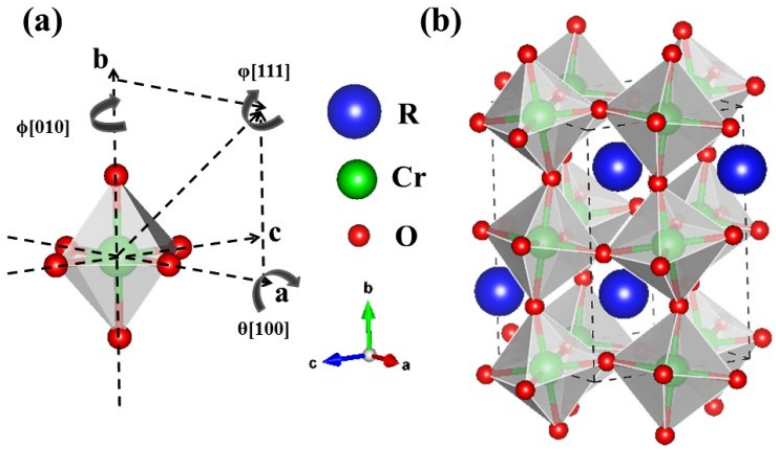

Figure 1. (a) shows the octahedral rotation along ϕ [010] and θ [100] which result in tilting φ [111] axes of regular octahedral, and (b) orthochromites $RCrO_3$ which has the structure of orthorhombic, with space group 62 (Pnma).

An extremely used parameter to quantify the stability and distortions of perovskite structures, as well as orthochromites, is the Goldschmidt tolerance factor (t) (Bhalla, Guo, & Roy, 2000; Goldschmidt, 1926), defined as:

$$t = \frac{r_R + r_O}{\sqrt{2}(r_{Cr} + r_O)} \quad (1)$$

where r_R is the radius of the R-cation (valence 3+), r_{Cr} is the radius of the Cr-cation (valence 3+) and r_O is the radius of the oxygen in six-coordination (valence -2). If $t = 1$, we have an ideal cubic perovskite, if we have between $0.75 < t < 1.0$ we have other structures such as the orthorhombic, however, if $t > 1$, it ceases to be perovskite.

In the orthochromites, the distortion mechanism is a tilting of rigid CrO_6 octahedron, as can be seen in Figure 1. From the crystallographic point of view, the inclination angles of the octahedral are directly related to $\langle Cr - O(1) - Cr \rangle$ and $\langle Cr - O(2) - Cr \rangle$, as shown in Figure 2. The first is the angle of inclination of the octahedron (θ) in relation to the plane [100], and the second is the angle of rotation (Φ) relative to the plane [010].

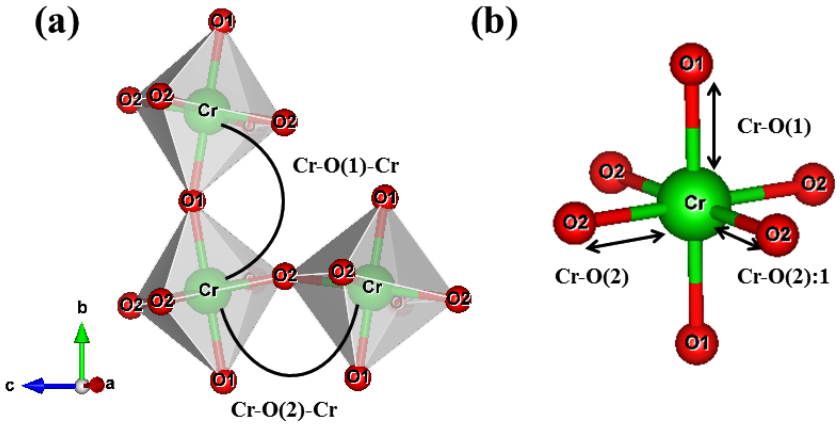

Figure 2. (a) $\langle Cr - O(1) - Cr \rangle$ and $\langle Cr - O(2) - Cr \rangle$ are bond angles of the octahedron, and (b) $Cr - O(1)$, $Cr - O(2)$ and $Cr - O(2)$: 1 bond lengths.

It is possible to observe in Figure 2: (a) $\langle Cr-O(1)-Cr\rangle$ and $\langle Cr-O(2)-Cr\rangle$ bond angles of the octahedron, and (b) $Cr-O(1)$, $Cr-O(2)$ and $Cr-O(2)$: 1 bond lengths. The octahedral tilt angles are defined by Zhao, Weidner, Parise and Cox (1993), as:

$$\theta = \frac{180-\langle Cr-O(1)-Cr\rangle}{2} \quad (2)$$

$$\cos(\Phi) = \frac{180-\langle Cr-O(1)-Cr\rangle}{2} / \sqrt{\cos(\theta)} \quad (3)$$

Another quantity used to quantify the distortion of the octahedron CrO_6 is the distortion parameter Δ_{oct} (Romero et al., 2015), which is defined as:

$$\Delta_{oct} = \frac{\sum\left|(Cr-O_i)-\langle Cr-O\rangle_{average}\right|}{\langle Cr-O\rangle_{average}} \quad (4)$$

where $\langle Cr-O\rangle_{average}$ is an average bond length.

Finally, using the XRD data, it was possible to estimate the Strain (ε) of the crystalline cell through the Williamson-Hall (W-H) method, which takes into account the distances at half height of the diffraction peaks (Rosenberg et al., 2000). W-H analysis proposes a diffraction line broadening due to crystallite size and strain contribution as a function of diffraction angle which can be written in the form of mathematical expression as $\beta_{hkl} = \beta_t + \beta_\varepsilon$ where β_t is due to crystallite size contribution, β_ε is due to strain-induced broadening and β_{hkl} is the full-width at half of the maximum intensity (FWHM) of instrumental corrected broadening (Dhahri, Dhahri, Dhahri, Taibi, & Hlil, 2017). Crystallite size contribution is calculated using the Scherrer equation:

$$D = \frac{k\lambda}{\beta_t \cos(\theta)} \quad (5)$$

The k constant depends upon the shape of the crystallite size ($k = 0.9$, assuming the circular grain), β_t is Full Width at Half Maximum (FWHM) of intensity vs. 2θ profile, λ is the wavelength of the Cu-K_α radiation (λ=*1.5406* Å) and θ is the Bragg diffraction angle. While the strain contribution is calculated by:

$$\beta_t = 4\varepsilon \tan(\theta) \quad (6)$$

where ε is the strain. We can see clearly that line broadening is a combination of crystallite size and strain, which is represented by the equation:

$$\beta_{hkl}\cos(\theta) = \frac{k\lambda}{D} + 4\varepsilon \sin(\theta) \quad (7)$$

This gives a linear relationship between βcos(θ) and 4sin(θ) when plotted as βcos(θ) (y-axis) vs. 4sin(θ) (x-axis). The crystallite size (D) can be calculated, by fitting Eq. (7), from the interception of the linear fit, and the value of Strain (ε) is calculated from the slope, which is also our interest in this work (Zak, Majid, Abrishami, & Yousefi, 2011).

Results and discussion

As previously mentioned, the values of the parameters used in this work were taken from the ICSD (793440), (251088) and (251108), for the samples $LaCrO_3$, $GdCrO_3$, and $YCrO_3$, respectively. The lattice parameters (*a,b,c*), unit cell volume (*V*) and the Goldschmidt tolerance factor (*t*), using the ionic radius of the $r_{La^{3+}}$= 1.03Å, $r_{Gd^{3+}}$= 0.96Å and $r_{Y^{3+}}$= 0.89Å, are shown in Table 1. The atomic positions are shown in Table 2, while the distortion parameter (Δ_{oct}) and the inclination (θ) and rotation (ϕ) angles of the octahedrons are shown in Table 3, for the orthochromites $RCrO_3$ (R = La, Gd, and Y).

Table 1. Lattice parameters (*a,b,c*), unit cell volume (*V*), the Goldschmidt tolerance factor (*t*), and R^{3+} ionic radius values (Shannon, 1976).

Structure	$r_R{}^{3+}$(Å)	a (Å)	b (Å)	c (Å)	V (Å3)	T
$LaCrO_3$	1.03	5.47883	7.75778	5.51493	234.40	0.85
$GdCrO_3$	0.96	5.52582	7.60635	5.31376	223.34	0.83
$YCrO_3$	0.89	5.52267	7.53555	5.24376	218.27	0.80

Table 2. Atomic positions of the orthochromites $RCrO_3$ (R = La, Gd, and Y).

Structure	Atom	*x*	*y*	*Z*
$LaCrO_3$	La	0.0200	0.2500	-0.0040
	O(1)	0.4930	0.2500	0.0610
	O(2)	0.2730	0.0360	0.7220
$GdCrO_3$	Gd	0.0585	0.2500	-0.0131
	O(1)	0.4680	0.2500	0.0980
	O(2)	0.2920	0.0010	0.0020
$YCrO_3$	Y	0.0666	0.2500	-0.0170
	O(1)	0.4652	0.2500	0.1044
	O(2)	0.3023	0.0538	-0.3073

Table 3. Geometrical parameters characterizing of the orthochromites $RCrO_3$ (R = La, Gd, and Y).

Bond length (Å)	$LaCrO_3$	$GdCrO_3$	$YCrO_3$
Cr-O(1)	1.969	1.980	1.971
Cr-O(2)	1.992	1.984	1.993
Cr-O(2):1	1.956	1.974	1.988
$\langle \boldsymbol{Cr-O} \rangle$	1.972	1.979	1.984
Δ_{oct}	0.019	0.006	0.013
Bond angle (°)	$LaCrO_3$	$GdCrO_3$	$YCrO_3$
$\langle \boldsymbol{Cr-O(1)-Cr} \rangle$	160.01	147.76	145.83
$\langle \boldsymbol{Cr-O(2)-Cr} \rangle$	160.32	151.26	146.04
θ [100]	9.99	16.12	17.09
cos(Φ) [010]	10.69	14.98	18.22

Figure 3 shows the graph of the lattice parameters (*a,b,c*), unit cell volume (*V*) and tolerance factor (*t*) as a function of the ionic radius (R^{3+} = La^{3+}, Gd^{3+} and Y^{3+}), data from Table 1. The *b* and *c* lattice parameters increased whereas *a* lattice parameter decreased, as the ionic radius of R^{3+} increased, as a consequence, an observation in an increased unit-cell volume. Also, the increase of the unit cell volume induces a Goldschmidt tolerance factor increase.

Figure 4 shows the graph of geometrical parameters that characterize the orthochromites as the $\langle Cr-O(1)-Cr \rangle$ and $\langle Cr-O(2)-Cr \rangle$ bond angles, distortion parameter (Δ_{oct}), inclination (θ), and rotation (ϕ) angles of the octahedrons, as a function of the ionic radius (R^{3+} = La^{3+}, Gd^{3+}, and Y^{3+}), data from Table 3. As can be seen, the $\langle Cr-O(1)-Cr \rangle$ and $\langle Cr-O(2)-Cr \rangle$ bond angles increase with an increase in the ionic radius, and wherefore the angle of inclination (θ), as well as rotation cos(Φ), tends to decrease with an increase in the ionic radius because they are inversely proportional. The distortion parameter (Δ_{oct}) suffers fluctuations in its values according to the increasing ionic radius, and this happens because it takes into consideration the same $Cr-O(1)$, $Cr-O(2)$ and $Cr-O(2)$: 1 bond lengths, as well as the same $\langle Cr-O \rangle$ average between them.

Figure 5 shows the adjustment of Williamson-Hall (W-H) using equation (7), which is plotted as a function of $\beta_{hkl}\cos(\theta)$ (y-axis) vs. $4\sin(\theta)$ (x-axis) for the $LaCrO_3$, $GdCrO_3$, and $YCrO_3$ structures. With the linear adjustment, it is possible to determine (estimate) the Strain (ε) value through the angular coefficient of the line for each sample. The values obtained for the Strain (ε) as well as its associated error (σ_ε) can be seen in Table 4.

As can be seen in Table 4, the strain value tends to decrease according to the decreasing ionic radius, that is, ε = 0.078, 0.069, and 0.062 for the $LaCrO_3$, $GdCrO_3$ and $YCrO_3$ structures, respectively. This result is related and in agreement with the volume of the unit cell, where we observe (see Table 1) that the volume decreases according to the decrease in the ionic radius, that is, the tensions of the crystalline unit cell tend to decrease due to the decrease of the lattice parameters so the strain also tends to decrease. This suggests, for example, that the $YCrO_3$ compound can accommodate doping or substitutions ions more easily in its structure, while $LaCrO_3$ (with a higher strain) is more subject to a structural phase transition in the same circumstance.

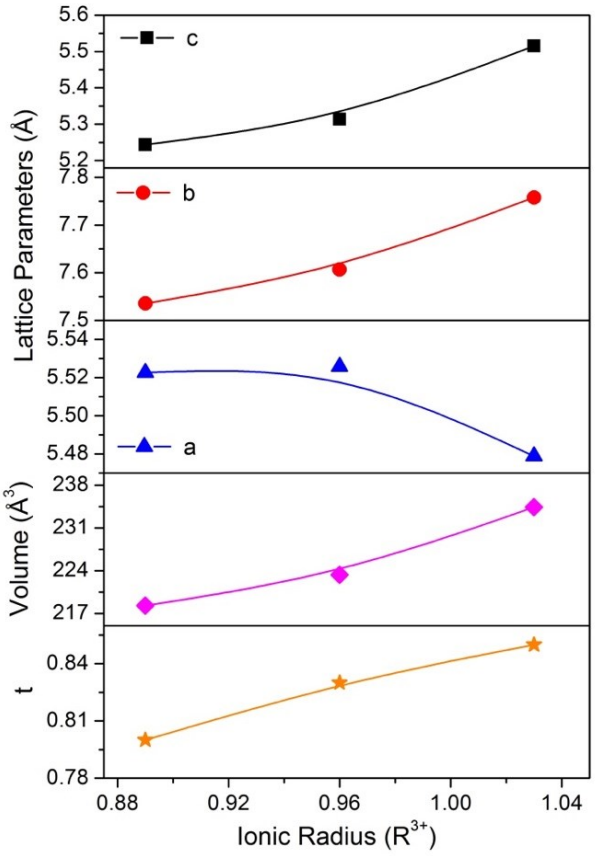

Figure 3. Graph of the lattice parameters (a,b,c), unit cell volume (V), and tolerance factor (t) as a function of the ionic radius.

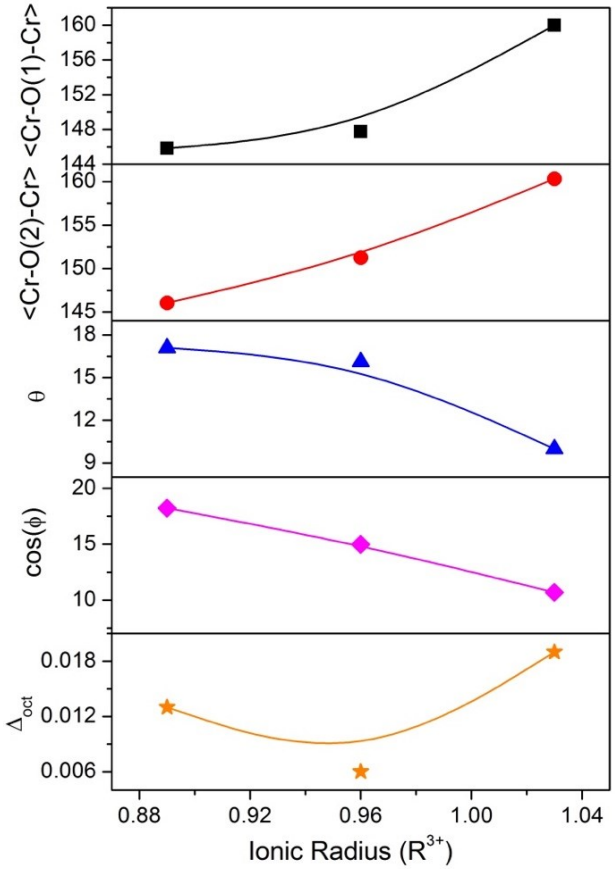

Figure 4. Graph of the $\langle Cr-O(1)-Cr\rangle$ and $\langle Cr-O(2)-Cr\rangle$ bond angles, distortion parameter (Δ_{oct}), inclination (θ), and rotation (ϕ) angle of the octahedron, as a function of the ionic radius.

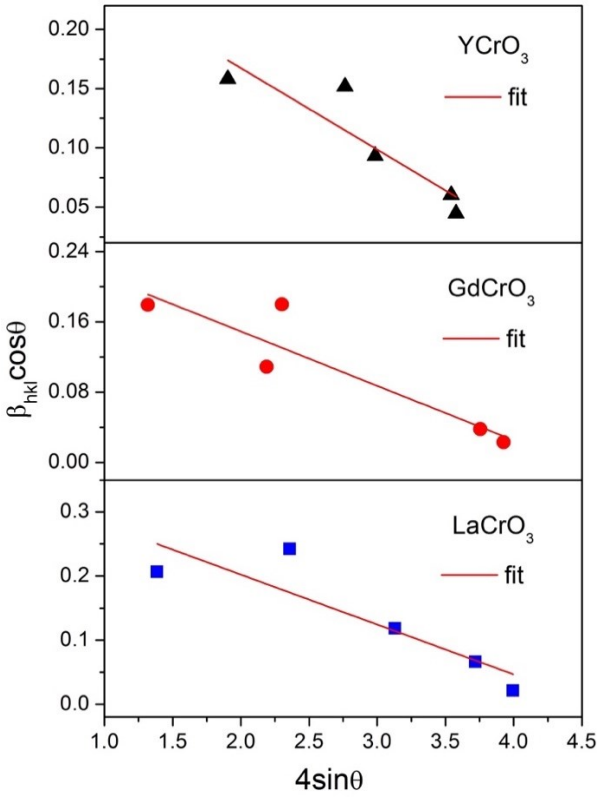

Figure 5. Graph of the fit of Williamson-Hall (W-H) for the $LaCrO_3$, $GdCrO_3$, and $YCrO_3$ structures.

Table 4. Strain (ε) values and error (σ_ε) obtained by linear adjustment for the $LaCrO_3$, $GdCrO_3$, and $YCrO_3$ structures.

Strain	$LaCrO_3$	$GdCrO_3$	$YCrO_3$
ε	0.078	0.069	0.062
σ_ε	0.023	0.015	0.018

Conclusion

In summary, was performed a comparative study of the effect of ionic radius on the structural properties of orthochromites $RCrO_3$ (R = La, Gd, and Y). It is observed that the *b* and *c* lattice parameters increase, whereas *a* lattice parameter decreased, as the ionic radius of R^{3+} increased, and by consequence, an increase in the unit-cell volume is observed. By analyzing the angles and bond lengths, the same increase with an increase in ionic radius, the inclination and rotation angles tend to decrease. The distortion parameter suffers fluctuation in its value according to the increased ionic radius. The strain for the orthochromites decreased according to the decrease in the ionic radius. Thence, the main objective of this work, which was to describe in detail how to obtain important parameters in the structural analysis of materials with perovskite structure, in order to help research beginners in this area, was achieved successfully.

Acknowledgements

The author thanks the support of the Brazilian funding agency of Coordenação de Aperfeiçoamento de Pessoal de Nível Superior – Capes (Finance Code-001).

References

Bhalla, A. S., Guo, R., & Roy, R. (2000). The perovskite structure – a review of its role in ceramic science and technology. *Materials Research Innovations, 4*(1), 3-26. doi: 10.1007/s100190000062

Dhahri, K., Dhahri, N., Dhahri, J., Taibi, K., & Hlil, E. K. (2017). Effect of (Al, Sn) doping on structural, magnetic and magnetocaloric properties of $La_{0.7}Ca_{0.1}Pb_{0.2}Mn_{1-x-y}Al_xSn_yO_3$ ($0 \leqslant x,y \leqslant 0.075$) manganites. *Journal of Alloys and Compounds*, *699*, 619-626. doi: 10.1016/j.jallcom.2016.12.324

Goldschmidt, V. M. (1926). Die Gesetze der Krystallochemie. *Naturwissenschaften*, *14*, 477-485. doi: 10.1007/BF01507527

Jara, A. N. L., Carvalho, J. F., Franco Júnior, A., Maia, L. J. Q., & Santana, R. C. (2018). On the optical and magnetic studies of $YCrO_3$ perovskites. *Physica B: Condensed Matter*, *546*, 67-72. doi: 10.1016/j.physb.2018.07.026

Oikawa, K., Kamiyama, T., Hashimoto, T., Shimojyo, Y., & Morii, Y. (2000). Structural phase transition of orthorhombic $LaCrO_3$ studied by neutron powder diffraction. *Journal of Solid State Chemistry*, *154*(2), 524-529. doi: 10.1006/jssc.2000.8873

Rajeswaran, B., Khomskii, D. I., Zvezdin, A. K., Rao, C. N. R., & Sundaresan, A. (2012). Field-induced polar order at the Néel temperature of chromium in rare-earth orthochromites: interplay of rare-earth and Cr magnetism. *Physical Review B*, *86*(21), 1-5. doi: 10.1103/PhysRevB.86.214409

Romero, M., Escamilla, R., Marquina, V., & Gómez, R. (2015). Structural and mechanic properties of $RFeO_3$ with R = Y, Eu, and La perovskites: a first-principles calculation. *The European Physical Journal D*, *69(7)*, 1-6. doi: 10.1140/epjd/e2015-60186-4

Rosenberg, Y., Machavariani, V. S., Voronel, A., Garber, S., Rubshtein, A., Frenkel, A. I., & Stern, E. A. (2000). Strain energy density in the x-ray powder diffraction from mixed crystals and alloys. *Journal of Physics: Condensed Matter*, *12*(37), 8081-8088. doi: 10.1088/0953-8984/12/37/307

Shannon, R. D. (1976). Revised effective ionic radii and systematic studies of interatomic distances in halides and chalcogenides. *Acta Crystallographica Section A*, *32*, 751-767. doi: 10.1107/S0567739476001551

Silva Jr., R. S., Aguiar, J. A., & Barrozo, P. (2018). Magnetization study in $LaCr_{1-x}Al_xO_3$ ($0 \leqslant x \leqslant 0.95$). *Ceramics International*, *44*(6), 5921-5925. doi: 10.1016/j.ceramint.2017.12.153

Warshi, M. K., Mishra, V., Sagdeo, A., Mishra, V., Kumar, R., & Sagdeo, P. R. (2018). Synthesis and characterization of $RFeO_3$: experimental results and theoretical prediction. *Advances in Materials and Processing Technologies*, *4*(4), 558–572. doi: 10.1080/2374068X.2018.1483680

Zak, A. K., Majid, W. H. A., Abrishami, M. E., & Yousefi, R. (2011). X-ray analysis of ZnO nanoparticles by Williamson-Hall and size-strain plot methods. *Solid State Sciences*, *13*(1), 251-256. doi: 10.1016/j.solidstatesciences.2010.11.024

Zhang, H., Wang, J., Xie, L., Fu, D., Guo, Y., & Li, Y. (2017). Reversal of spontaneous magnetization and spontaneous exchange bias for $Sm_{1-x}Y_xCrO_3$: The effect of Y doping. *Journal of Applied Physics*, *122*(20), 1-7. doi: 10.1063/1.4995459

Zhao, Y., Weidner, D. J., Parise, J. B., & Cox, D. E. (1993). Thermal expansion and structural distortion of perovskite – data for $NaMgF_3$ perovskite. Part I. *Physics of the Earth and Planetary Interiors*, 76(1-2), 1-16. doi: 10.1016/0031-9201(93)90051-A